

Surface structures of binary mixtures of imidazolium-based ionic liquids using high-resolution Rutherford backscattering spectroscopy and time of flight secondary ion mass spectroscopy

Kaoru Nakajima, Motoki Miyashita, Motofumi Suzuki, and Kenji Kimura

Citation: [The Journal of Chemical Physics](#) **139**, 224701 (2013); doi: 10.1063/1.4838376

View online: <http://dx.doi.org/10.1063/1.4838376>

View Table of Contents: <http://scitation.aip.org/content/aip/journal/jcp/139/22?ver=pdfcov>

Published by the [AIP Publishing](#)



Re-register for Table of Content Alerts

Create a profile.



Sign up today!



Surface structures of binary mixtures of imidazolium-based ionic liquids using high-resolution Rutherford backscattering spectroscopy and time of flight secondary ion mass spectroscopy

Kaoru Nakajima, Motoki Miyashita, Motofumi Suzuki, and Kenji Kimura^{a)}

Department of Micro Engineering, Kyoto University, Kyoto-daigaku-Katsura, Nishikyo, Kyoto 615-8549, Japan

(Received 5 October 2013; accepted 19 November 2013; published online 9 December 2013)

Surface structures of binary mixtures of imidazolium-based ionic liquids having a common anion (bis(trifluoromethanesulfonyl)imide ([TFSI]), namely $[C_2MIM]_{1-x}[C_{10}MIM]_x[TFSI]$ ($x = 0.5$ and 0.1), are studied using high-resolution Rutherford backscattering spectroscopy (HRBS) and time of flight secondary ion mass spectroscopy (TOF-SIMS). Although both measurements show surface segregation of $[C_{10}MIM]$ the degrees of the segregation are different. The surface fraction x_{surf} of $[C_{10}MIM]$ is estimated to be 0.6 ± 0.05 and 0.18 ± 0.02 by HRBS for $x = 0.5$ and 0.1 , respectively. On the other hand, TOF-SIMS indicates much stronger surface segregation, namely $x_{surf} = 0.83 \pm 0.03$ and 0.42 ± 0.04 for $x = 0.5$ and 0.1 , respectively. The observed discrepancy can be attributed to the difference in the probing depth between HRBS and TOF-SIMS. The observed surface segregation can be roughly explained in terms of surface tension. © 2013 AIP Publishing LLC. [<http://dx.doi.org/10.1063/1.4838376>]

I. INTRODUCTION

Room-temperature ionic liquids (ILs) are often called as “designer solvents” because the properties of ILs can be tuned by choosing an appropriate combination of a wide range of cations and anions. This allows a variety of promising applications.^{1–8} The concept of designer solvents can be extended by using mixtures of different ILs to tune the properties more finely.⁹ Recently, it has been recognized that not only the bulk properties but also the surface properties, such as surface tension, wettability, heat and mass transport, are of prime importance for a number of applications.^{10–13} In this context, understanding of the surface structures of ILs is of prime importance. Many surface analysis techniques, such as direct recoil spectroscopy,¹⁴ sum frequency generation (SFG) spectroscopy,¹⁵ X-ray reflectivity (XR) measurement,¹⁶ angle resolved X-ray photoelectron spectroscopy (ARXPS),¹⁷ low energy ion scattering spectroscopy (LEIS),¹⁸ metastable impact electron spectroscopy (MIES),¹⁹ time of flight secondary ion mass spectroscopy (TOF-SIMS),²⁰ high-resolution Rutherford backscattering spectroscopy (HRBS)²¹ and Neutral impact collision ion scattering spectroscopy (NICISS),²² have been employed to study the surface structures of ILs. These techniques have their own pros and cons. In the early days, there were discrepancies between the observed surface structures.^{14–16} After extensive studies, a general consensus has been formed on the surface structures of ILs.¹³ The surface is shared equally between cations and anions. When the molecules contain alkyl chains, the alkyl chains protrude into the vacuum. Concerning the surface structures of mixtures of ILs, however, there are still conflicting results.

Souda has studied the surface composition of binary mixtures of ILs using TOF-SIMS.²³ He found very strong surface segregation of larger cations and/or larger anions. This suggests that the surface properties can be designed separately from the bulk properties by using mixtures of appropriate ILs. We have also observed the surface structures of equimolar mixtures of imidazolium-based ionic liquids (ILs) having a common cation (1-butyl-3-methylimidazolium ($[C_4MIM]$) or 1-hexyl-3-methylimidazolium ($[C_6MIM]$)) and different anions (bis(trifluoromethanesulfonyl)imide ([TFSI]), hexafluorophosphate ($[PF_6]$) or chlorine) using HRBS.²⁴ Our results, however, are very different from the TOF-SIMS result. We found that the [TFSI] anion is slightly enriched at the surface relative to $[PF_6]$ with coverage of $\sim 60\%$ for the equimolar mixtures of $[C_{4(6)}MIM][TFSI]_{0.5}[PF_6]_{0.5}$. No surface segregation is observed for $[C_6MIM][TFSI]_{0.5}[Cl]_{0.5}$ and $[C_6MIM][PF_6]_{0.5}[Cl]_{0.5}$. This is very different from the TOF-SIMS result. A similar result (no surface segregation) was also observed for the mixture of $[C_2MIM][TFSI]$ and $[C_{12}MIM][TFSI]$ using ARXPS.²⁵ The origin of the discrepancy between TOF-SIMS and HRBS/ARXPS has not been clarified yet.

In the present paper, we observe the surface structure of the mixture of $[C_2MIM][TFSI]$ and $[C_{10}MIM][TFSI]$ using HRBS and TOF-SIMS. The result of HRBS shows weak surface segregation of $[C_{10}MIM]$ while the TOF-SIMS result shows rather strong surface segregation of $[C_{10}MIM]$. The origin of the observed discrepancy is discussed based on the surface structures observed by HRBS.

II. EXPERIMENTAL

The ILs used in this study were purchased from Kanto Reagent (Japan) and measured by HRBS and TOF-SIMS

^{a)} Author to whom correspondence should be addressed. Electronic mail: kimura@kues.kyoto-u.ac.jp

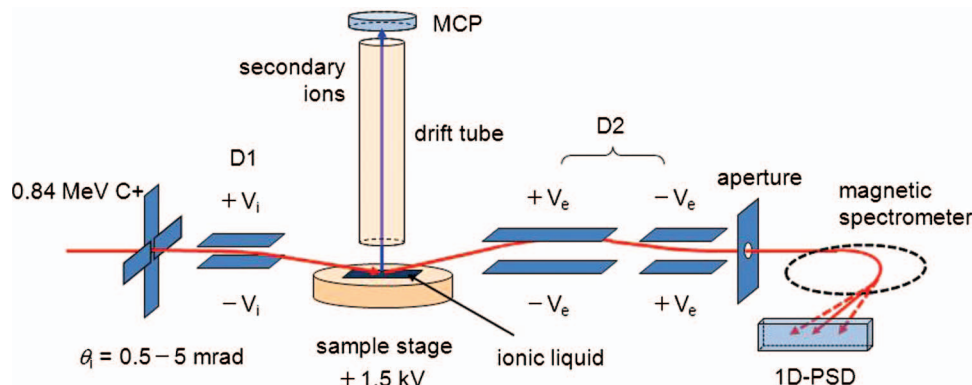


FIG. 1. Schematic drawing of the TOF-SIMS setup.

without further purification. The details of the HRBS measurement can be found in our previous papers.^{24,26} A schematic drawing of the TOF-SIMS setup is shown in Fig. 1. A disk-shaped sample holder made of copper was filled with IL and kept for a few days in an UHV scattering chamber (base pressure 2×10^{-8} Pa) before SIMS measurements to reduce possible contamination of water. The UHV chamber was connected to the 4 MV Van de Graaff accelerator of Kyoto University via a differential pumping system. A beam of 0.84 MeV C^+ ions was collimated by a series of 4-jaw slit systems to 0.1×0.1 mm² in size and less than 0.2 mrad in divergence. The beam current was monitored by a Faraday cup. The beam current was reduced lower than the detection limit of the Faraday cup (<0.1 pA) during the TOF-SIMS measurement. The collimated beam was slightly deflected downwards using an electrostatic deflector installed just before the sample holder so that the C^+ ions were incident on the surface of IL at a grazing angle. There are a couple of electrostatic deflectors downstream the target. By applying appropriate voltages on these deflectors the ions scattered at a chosen scattering angle were selected by a small aperture (acceptance angle ± 1.1 mrad) placed on the entrance focal plane of a 90° sector magnetic spectrometer. Using this system energy spectrum of the scattered ions at scattering angles ranging from 0 to 10 mrad can be measured without rotating the magnetic spectrometer around the target. The energy resolution of the spectrometer was about 1 keV for 0.84 MeV C^+ ions. The secondary ions emitted from the surface of IL were accelerated to 1.5 keV and detected by a micro-channel plate (MCP) after traveling a drift tube of 410 mm length. Using the signals of the scattered C ions detected by the 90° magnetic spectrometer as start signals, the time of flight spectrum of the secondary ions was measured. Note that the incident C^+ ions are subject to charge exchange processes during the scattering from the IL. We measured C^{2+} ions using the magnetic spectrometer because C^{2+} is the dominant charge state under the present conditions. This grazing incidence SIMS provides excellent surface sensitivity because the scattered ions interact only with the surface region as is discussed later in this paper. It should be noted that the estimated intensity of the primary ion beam is $<1 \times 10^4$ ions/s and the typical measurement time is 1 h. This corresponds to a fluence of $<1 \times 10^{10}$ ions/cm², which is four orders of magnitude smaller than the surface density of molecules. Thus the radiation damage induced by

the primary ions can be neglected in the present TOF-SIMS measurement.

III. RESULTS

A. HRBS measurement

Figure 2 shows examples of the HRBS spectra observed at an exit angle $\theta_e = 87^\circ$ with respect to the surface normal, when 400 keV He^+ ions were incident on $[C_2MIM][TFSI]$, $[C_{10}MIM][TFSI]$, and equimolar mixture of $[C_2MIM]_{0.5}[C_{10}MIM]_{0.5}[TFSI]$. There are several steps in the observed spectra. Each step corresponds to the onset of the spectrum of each element, namely, the step corresponds to the surface position of each element. The dashed lines show the results of the spectrum simulation for a uniform and stoichiometric composition. The agreement between the measurement and the simulation is roughly good, showing that the overall composition is close to the stoichiometric composition. Looking at the spectrum closely, however, the observed spectra deviate from the simulated ones around the steps. For example, a sharp peak is seen

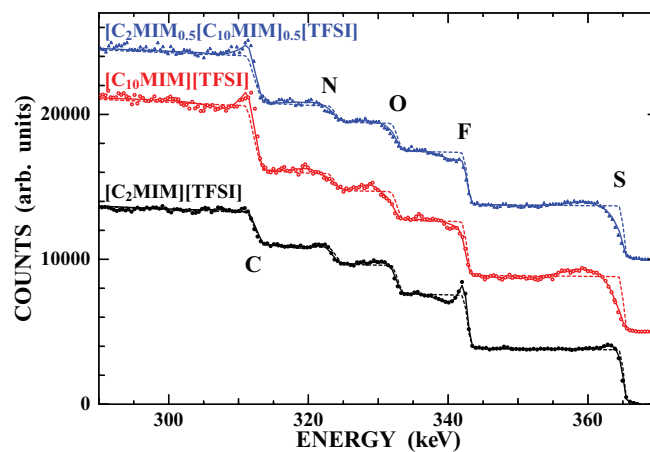


FIG. 2. HRBS spectra of $[C_2MIM][TFSI]$, $[C_{10}MIM][TFSI]$, and $[C_2MIM]_{0.5}[C_{10}MIM]_{0.5}[TFSI]$ observed at an exit angle $\theta_e = 87^\circ$ with respect to the surface normal. The incident energy was 400 keV and the scattering angle is $\sim 50^\circ$. The dashed lines show the calculated spectra for a uniform and stoichiometric composition. The agreement between the observed and calculated spectra is reasonably good except for small discrepancies seen at the leading edges of elements. The solid lines show the best-fit results of spectrum simulation.

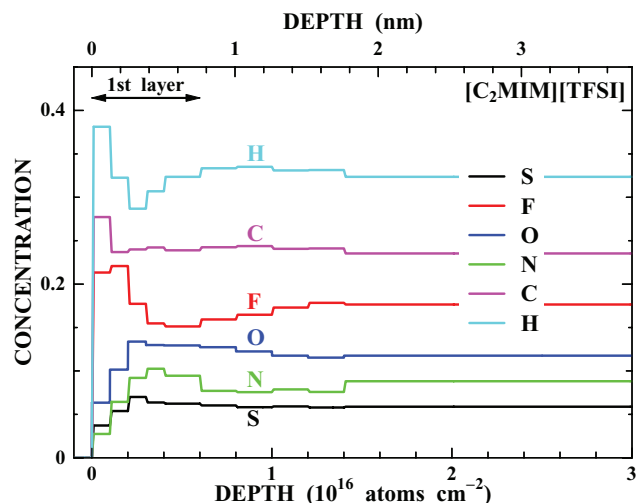


FIG. 3. Composition depth profiles for $[\text{C}_2\text{MIM}][\text{TFSI}]$ derived from the observed HRBS spectrum through spectrum simulation. The depth scale shown in the upper abscissa is calculated using a bulk density. The horizontal arrow shows the depth region corresponding to the topmost molecular layer estimated using the bulk density.

at the fluorine edge for $[\text{C}_2\text{MIM}][\text{TFSI}]$, similar peaks are also seen at the carbon edge for $[\text{C}_{10}\text{MIM}][\text{TFSI}]$ and $[\text{C}_2\text{MIM}]_{0.5}[\text{C}_{10}\text{MIM}]_{0.5}[\text{TFSI}]$. These deviations indicate that the surface composition is different from the bulk composition and/or the molecules have preferential orientations.

The composition depth profiles were derived through the spectrum simulation. The best-fit result of the spectrum simulation is shown by solid lines in Fig. 2. The obtained composition depth profiles are shown in Figs. 3–5. It should be noted that the RBS analysis gives the depth scale in units of areal density of atoms (i.e., atoms cm^{-2}). This depth scale can be converted to “nm” using the bulk density of IL as is shown in the upper abscissa. Note that the scale in nm is just a rough estimate because the atomic density might be different from the

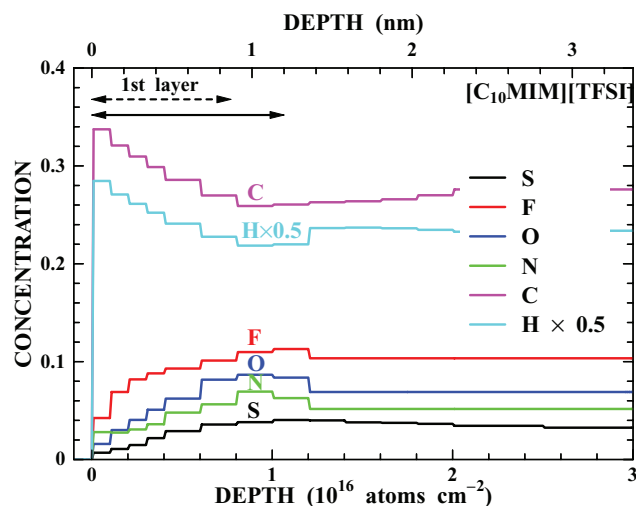


FIG. 4. Composition depth profiles for $[\text{C}_{10}\text{MIM}][\text{TFSI}]$ derived from the observed HRBS spectrum through spectrum simulation. The depth scale shown in the upper abscissa is calculated using a bulk density. The dashed arrow shows the depth region corresponding to the topmost molecular layer estimated using the bulk density. The solid arrow shows that estimated from SFG results (see text).

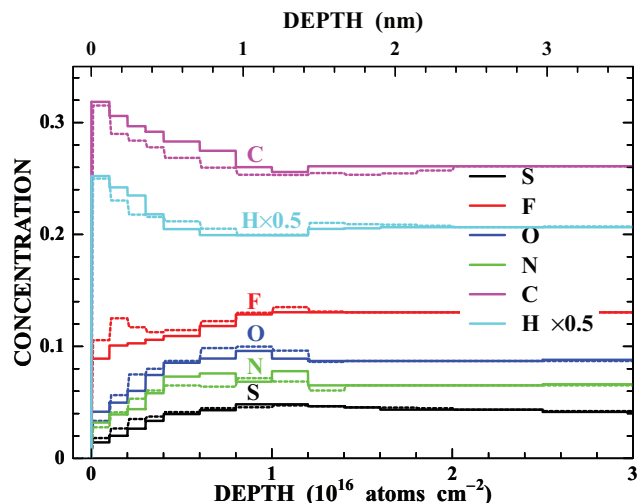


FIG. 5. Composition depth profiles for $[\text{C}_2\text{MIM}]_{0.5}[\text{C}_{10}\text{MIM}]_{0.5}[\text{TFSI}]$ derived from the observed HRBS spectrum through spectrum simulation (solid lines). The depth scale shown in the upper abscissa is calculated using a bulk density. The dashed lines show the averaged profiles of $[\text{C}_2\text{MIM}][\text{TFSI}]$ and $[\text{C}_{10}\text{MIM}][\text{TFSI}]$ (see text).

bulk density in the surface region. We also mention that the depth resolution of HRBS is about 0.1 nm at the surface in the present case and becomes worse with increasing depth due to energy loss straggling, for example, the depth resolution becomes about 1 nm at a depth of 3 nm. From these figures it is clear that the observed composition deviates from the bulk composition at surface although the agreement is very good at the deeper region.

The thickness of one molecular layer can be estimated by $t = \rho^{-1/3}$, where ρ is the bulk density of molecular pair (2.34×10^{21} and $1.53 \times 10^{21} \text{ cm}^{-3}$ for $[\text{C}_2\text{MIM}][\text{TFSI}]$ and $[\text{C}_{10}\text{MIM}][\text{TFSI}]$, respectively). The estimated thickness is 0.75 nm for $[\text{C}_2\text{MIM}][\text{TFSI}]$. The depth region corresponding to the topmost molecular layer is shown by a horizontal arrow in Fig. 3. By integrating the elemental depth profiles in this topmost molecular layer, the average composition in the topmost molecular layer was estimated to be $\text{S}_{2.0}\text{F}_{6.0}\text{O}_{3.9}\text{N}_{2.7}\text{C}_{8.3}$ for $[\text{C}_2\text{MIM}][\text{TFSI}]$. This is close to the stoichiometric composition, $\text{S}_2\text{F}_6\text{O}_4\text{N}_3\text{C}_8$, indicating that the surface is equally shared by cations and anions. However, the observed composition profiles are not flat in the topmost molecular layer, indicating that the molecules have preferential orientations at the surface. There are a small carbon peak at the surface and a large fluorine peak at ~ 0.1 nm while other elements are slightly depleted at the very surface region. These results indicate that the ethyl groups in the $[\text{C}_2\text{MIM}]$ cations and CF_3 groups in the $[\text{TFSI}]$ anions point toward the vacuum as is schematically shown in Fig. 6(a). This is in accordance with the previous studies.^{25,27} Note that $[\text{TFSI}]$ has two stable conformers, cis and trans conformers, and the latter is more stable than the former by 3.5 kJ mol^{-1} .²⁸ The fluorine profile has a sharp surface peak and a broad dip in the sub surface region. As was discussed in the previous paper, this fluorine profile indicates that cis conformer is dominant in the topmost molecular layer as is shown in Fig. 6(a).²⁷ This is reasonable because all CF_3 groups can occupy the surface to reduce the surface energy.

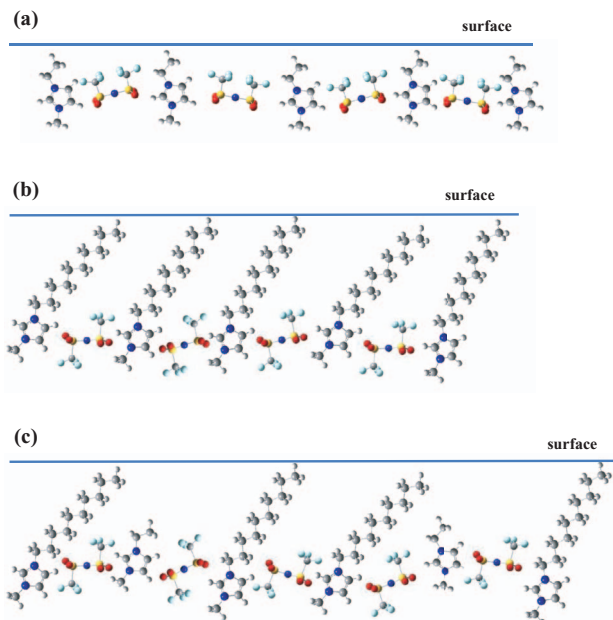


FIG. 6. Schematic drawings of the surface structures of (a) $[\text{C}_2\text{MIM}][\text{TFSI}]$, (b) $[\text{C}_{10}\text{MIM}][\text{TFSI}]$ and (c) mixture of $[\text{C}_2\text{MIM}]_{0.5}[\text{C}_{10}\text{MIM}]_{0.5}[\text{TFSI}]$.

As can be seen in Fig. 4, the elemental depth profiles of $[\text{C}_{10}\text{MIM}][\text{TFSI}]$ also deviate from the bulk composition in the surface region. The carbon profile has a broad surface peak while nitrogen is depleted in the surface region. This indicates that the decyl group points toward the vacuum. The profiles of oxygen and sulfur are very similar to nitrogen, showing that the $\text{N}(\text{SO}_2)_2$ moiety of $[\text{TFSI}]$ are located at almost the same depth as the imidazolium rings. On the other hand, the fluorine profile is slightly shifted to the vacuum compared with sulfur, oxygen, and nitrogen. This indicates that the CF_3 groups in $[\text{TFSI}]$ point toward the vacuum. Different from $[\text{C}_2\text{MIM}][\text{TFSI}]$, the fluorine profile does not have a sharp surface peak and is depleted in the surface region. This means that the CF_3 groups do not occupy the surface and the surface is covered by decyl chains. This suggests that the trans conformer of $[\text{TFSI}]$, which is energetically more stable than the cis conformer, is dominant. From these findings the surface structure of $[\text{C}_{10}\text{MIM}][\text{TFSI}]$ is derived as is shown in Fig. 6(b). This is again in good agreement with the results of the previous studies on $[\text{C}_n\text{MIM}][\text{TFSI}]$.^{25,27}

The thickness of one molecular layer was estimated to be 0.87 nm for $[\text{C}_{10}\text{MIM}][\text{TFSI}]$ using $t = \rho^{-1/3}$ (shown by a dashed arrow in Fig. 4). The average composition of the topmost molecular layer was estimated to be $\text{S}_{1.3}\text{F}_{4.8}\text{O}_{3.0}\text{N}_{2.3}\text{C}_{17.2}$, which deviates remarkably from the bulk composition $\text{S}_2\text{F}_6\text{O}_4\text{N}_3\text{C}_{16}$. This is because the simple estimate of the thickness of the topmost molecular layer ($t = \rho^{-1/3}$) is not correct for the ILs containing long molecules like $[\text{C}_{10}\text{MIM}]$ whose length is as long as ~ 1.8 nm. SFG measurements demonstrated that the alkyl chains of the surface $[\text{C}_n\text{MIM}]$ cations are tilted by $\sim 50^\circ$ with respect to the surface normal.^{29,30} Thus, the thickness of the topmost molecular layer of $[\text{C}_{10}\text{MIM}][\text{TFSI}]$ would be 1.2 nm (shown by a solid arrow in Fig. 4, which corresponds to 1.07×10^{16} atoms/cm²). Using the thickness thus estimated the average com-

position in the topmost molecular layer is estimated to be $\text{S}_{1.6}\text{F}_{5.3}\text{O}_{3.6}\text{N}_{2.8}\text{C}_{16.6}$ from the observed composition depth profile. This is in reasonable agreement with the bulk composition. It is noteworthy that sulfur, fluorine, oxygen, and nitrogen profiles have a peak around 1 nm. Because these elements are located at the bottom of the topmost molecular layer (see Fig. 6(b)) this is consistent with the above estimated thickness of 1.2 nm. This confirms that the decyl chains are tilted by $\sim 50^\circ$ at the surface of $[\text{C}_{10}\text{MIM}][\text{TFSI}]$.

Figure 5 shows the composition depth profiles of the mixture of $[\text{C}_2\text{MIM}]_{0.5}[\text{C}_{10}\text{MIM}]_{0.5}[\text{TFSI}]$ derived from the HRBS measurement. From these profiles, the composition of the topmost molecular layer is calculated to be $\text{S}_{1.5}\text{F}_{5.0}\text{O}_{3.4}\text{N}_{2.7}\text{C}_{13.3}$. For comparison, the averaged profiles of $[\text{C}_2\text{MIM}][\text{TFSI}]$ and $[\text{C}_{10}\text{MIM}][\text{TFSI}]$ (equal-weighted average) are also shown by dashed lines. The observed profiles of the mixture are expected to agree with these averaged profiles if there is no surface segregation of particular molecules. The agreement is very good at deeper region (>2 nm). In the region of the topmost molecular layer, however, there are discrepancies. For example, the observed carbon composition is larger than the averaged profile. This suggests surface segregation of $[\text{C}_{10}\text{MIM}]$.

In order to estimate the degree of the surface segregation quantitatively, the expected profiles for $[\text{C}_2\text{MIM}]_{1-x}[\text{C}_{10}\text{MIM}]_x[\text{TFSI}]$ were derived for various x by averaging the profiles of $[\text{C}_2\text{MIM}][\text{TFSI}]$ and $[\text{C}_{10}\text{MIM}][\text{TFSI}]$ with weights $1-x$ and x . From these weighted average profiles, the composition of the topmost molecular layer was calculated. Figure 7 shows the comparison between the composition thus calculated and the composition measured for the mixture ($\text{S}_{1.5}\text{F}_{5.0}\text{O}_{3.4}\text{N}_{2.7}\text{C}_{13.3}$). The abscissa shows x , the fraction of $[\text{C}_{10}\text{MIM}][\text{TFSI}]$, and the ordinate shows the ratio of the calculated composition to the measured one for each element. The fraction x_{surf} of the topmost molecular layer was determined for each element so that the ratio is equal to unity.

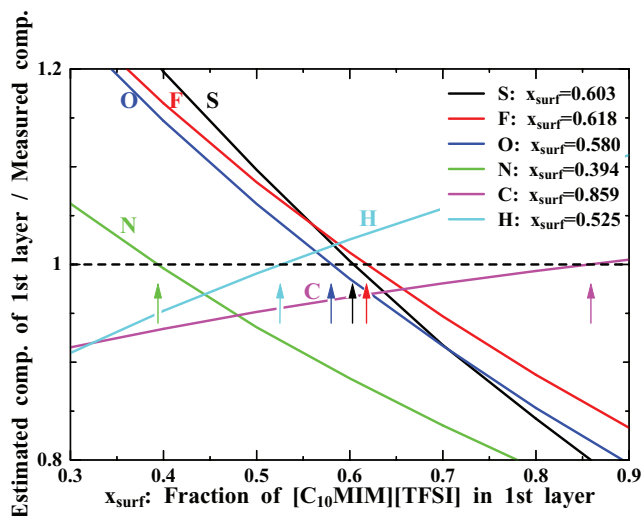


FIG. 7. Comparison between the estimated composition of the 1st layer with the measured one for $[\text{C}_2\text{MIM}]_{0.5}[\text{C}_{10}\text{MIM}]_{0.5}[\text{TFSI}]$. The ratio of the estimated composition to the measured one is shown for each element as a function of the $[\text{C}_{10}\text{MIM}]$ fraction, x_{surf} . The determined values of x_{surf} for each element are indicated (see text).

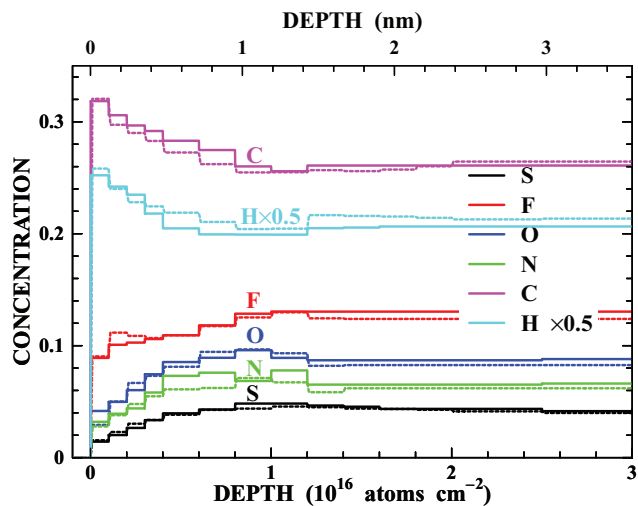


FIG. 8. Estimated depth profiles for $[\text{C}_2\text{MIM}]_{0.4}[\text{C}_{10}\text{MIM}]_{0.6}[\text{TFESI}]$ (dashed lines) are compared with the observed profiles for $[\text{C}_2\text{MIM}]_{0.5}[\text{C}_{10}\text{MIM}]_{0.5}[\text{TFESI}]$. The agreement is roughly good in the topmost molecular layer, indicating that a weak surface segregation of $[\text{C}_{10}\text{MIM}]$ occurs. Slight difference indicates the surface structure of the mixture is modified from a simple combination of pure ILs (see text).

The results are scattered in a rather wide region from 0.4 to 0.9, especially the results of light elements, as is shown in Fig. 7. This is because the precision of RBS analysis for light elements is generally poor compared to heavier elements due to their smaller cross sections and spectrum overlapping with heavier elements. The fraction averaged for all elements is $x_{\text{surf}} = 0.6 \pm 0.05$ and the same result ($x_{\text{surf}} = 0.6$) is also obtained by neglecting the light elements (H, C, N).

Figure 8 shows the comparison between the profiles expected for $[\text{C}_2\text{MIM}]_{0.4}[\text{C}_{10}\text{MIM}]_{0.6}[\text{TFESI}]$ (dashed lines) and the profiles measured for the mixture of $[\text{C}_2\text{MIM}]_{0.5}[\text{C}_{10}\text{MIM}]_{0.5}[\text{TFESI}]$ (solid lines). The agreement is improved substantially compared to Fig. 5. There are, however, still some differences. The estimated fluorine profile has a small peak at 0.2 nm while there is no such a peak in the measured profile. This suggests that $[\text{TFESI}]$, probably together with $[\text{C}_2\text{MIM}]$, are located deeper positions compared with the pure $[\text{C}_2\text{MIM}][\text{TFESI}]$ as is schematically shown in Fig. 6(c). In passing, we also estimated the elemental depth profiles of the mixture, aligning the observed profiles of pure ILs not from the surface but at the anion (and the cation core) positions. The obtained surface fraction x_{surf} is almost the same as obtained above.

A mixture of $[\text{C}_2\text{MIM}]_{0.9}[\text{C}_{10}\text{MIM}]_{0.1}[\text{TFESI}]$ was also measured by HRBS. Figure 9 shows the composition depth profiles determined from the observed HRBS spectrum. A similar analysis was done and the resultant fraction of the topmost molecular layer is $x_{\text{surf}} = 0.18 \pm 0.02$. The composition depth profiles expected for $[\text{C}_2\text{MIM}]_{0.82}[\text{C}_{10}\text{MIM}]_{0.18}[\text{TFESI}]$ (dashed lines) are compared with the observed profiles in Fig. 9. Similarly to Fig. 8, there are some discrepancies, i.e., the expected fluorine profile has a sharp peak at surface while the observed fluorine profile has a broad peak at slightly deeper position. The expected profiles for sulfur, oxygen, and nitrogen are shifted to the surface compare to the observed profiles. These differences are again attributed to the

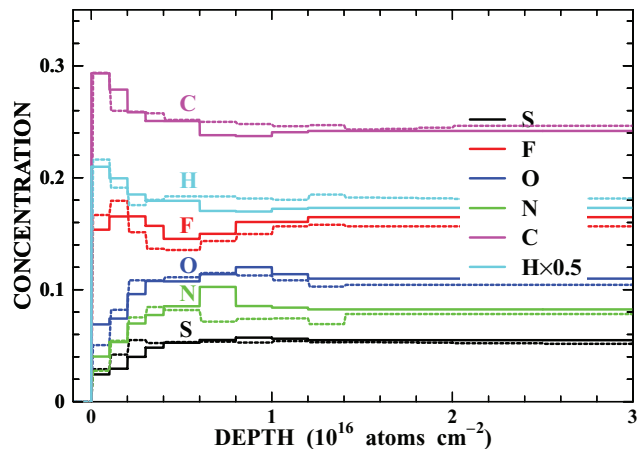


FIG. 9. Estimated depth profiles for $[\text{C}_2\text{MIM}]_{0.82}[\text{C}_{10}\text{MIM}]_{0.18}[\text{TFESI}]$ (dashed lines) are compared with the observed profiles for $[\text{C}_2\text{MIM}]_{0.9}[\text{C}_{10}\text{MIM}]_{0.1}[\text{TFESI}]$. The agreement is roughly good in the topmost molecular layer, indicating that a weak surface segregation of $[\text{C}_{10}\text{MIM}]$ occurs. Slight difference indicates the surface structure of the mixture is modified from a simple combination of pure ILs (see text).

fact that $[\text{TFESI}]$ and $[\text{C}_2\text{MIM}]$ molecules are located deeper positions compared with the pure $[\text{C}_2\text{MIM}][\text{TFESI}]$. The differences are more pronounced in the present case, because $[\text{C}_2\text{MIM}][\text{TFESI}]$ is dominant.

B. TOF-SIMS measurement

Figure 10 shows an example of the observed angular distribution of the scattered C^{2+} ion when 0.84 MeV C^+ ions are incident on $[\text{C}_2\text{MIM}][\text{TFESI}]$ at $\theta_i = 1.7$ mrad. The observed distribution has a well-defined peak at a scattering angle $\theta_s = 5.4$ mrad, which is slightly larger than the specular angle. Figure 11 shows the energy spectrum of the scattered C^{2+} ions observed at $\theta_s = 4.4$ mrad when 0.84 MeV C^+ ions are incident on $[\text{C}_2\text{MIM}][\text{TFESI}]$ at $\theta_i = 0.8$ mrad. For comparison the energy spectrum of the incident ions is also shown. The average energy loss of the scattered ions is calculated to be

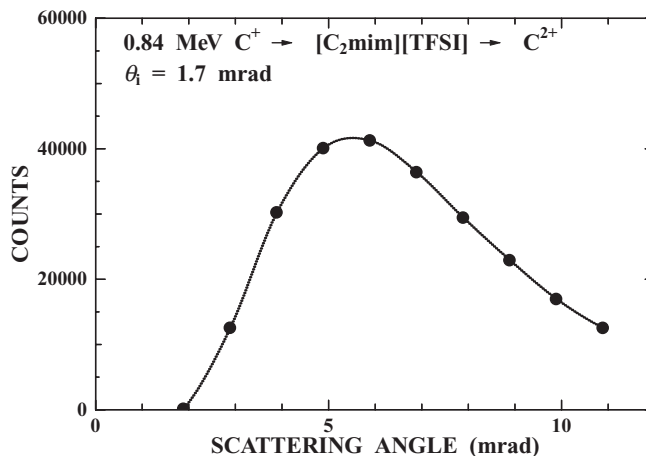


FIG. 10. Angular distribution of the scattered C^{2+} ions when 0.84 MeV C^+ ions are incident on $[\text{C}_2\text{MIM}][\text{TFESI}]$ at $\theta_i = 1.7$ mrad. The observed distribution has a well-defined peak at a scattering angle $\theta_s = 5.4$ mrad, which is slightly larger than the specular angle.

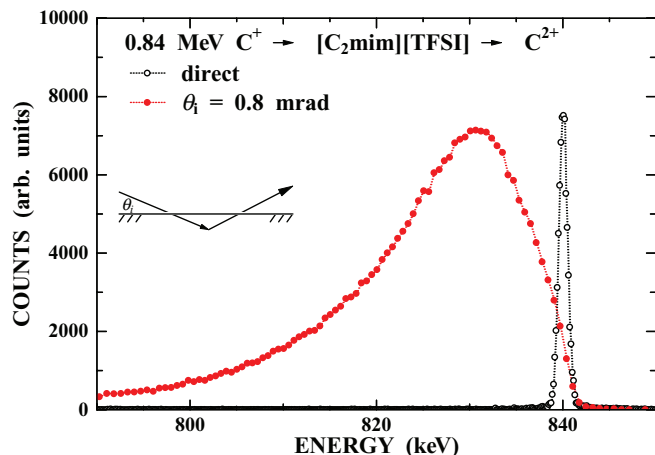


FIG. 11. The energy spectrum of the C^{2+} ions scattered at $\theta_s = 4.4$ mrad when 0.84 MeV C^+ ions are incident on $[C_2MIM][TFSI]$ at $\theta_i = 0.8$ mrad. The spectrum of the direct beam is also shown by open circles.

$\Delta E = 15.3$ keV. The stopping power S of 0.84 MeV C^+ ions in $[C_2MIM][TFSI]$ was calculated to be 0.64 keV/nm using SRIM code.³¹ Assuming that the ion trajectory can be approximated by two straight lines with a single deflection (see the inset of Fig. 11), the penetration depth is given by

$$d = \frac{\Delta E}{S \left(\frac{1}{\sin \theta_i} + \frac{1}{\sin(\theta_s - \theta_i)} \right)}. \quad (1)$$

The typical penetration depth in the present measurements is as small as ~ 0.05 nm. This does not mean that the information depth is 0.05 nm because the collision cascade may extend to several nm from the ion trajectory. However, such a small penetration depth indicates that the projectile energy is effectively transferred to the surface region. As a result, efficient secondary ion emission is expected.

Figure 12(a) shows an example of the observed TOF spectrum of the secondary ions emitted from $[C_2MIM][TFSI]$ during the grazing angle scattering of 0.84 MeV C^+ at $\theta_i = 0.8$ mrad. There are many peaks of secondary ions. The total secondary ion yield is calculated to be 0.7 ions per incident C^+ ion. This is extremely large compared with the conventional TOF-SIMS, where several tens keV ions are incident on a specimen at a large incident angle. This is partly because our probe ion interacts mainly with the surface. As a result, the energy of the probe ion is efficiently transferred to the surface molecules.

In the TOF spectrum, there is a relatively large peak of the intact cations ($[C_2MIM]^+$) at $m/q = 111$ as well as fragment ions such as CH_3^+ ($m/q = 15$), $C_2H_4^+$ ($m/q = 28$) and $C_2NH_4^+$ ($m/q = 42$) originating from the $[C_2MIM]$ cation. The yield of the intact $[C_2MIM]^+$ is 0.014 ions per incident ion. Concerning the $[TFSI]$ anion, no intact $[TFSI]$ ion was observed but some fragment ions, such as F^+ , CF^+ , and CF_3^+ are clearly seen at $m/q = 19$, 31, and 69, respectively.

Figure 12(b) shows the observed TOF spectrum of the secondary ions emitted from $[C_{10}MIM][TFSI]$ during the grazing angle scattering of 0.84 MeV C^+ at $\theta_i = 1.4$ mrad. There is a weak peak of $[C_{10}MIM]^+$ at $m/q = 223$ as well as fragment ions originating from $[C_{10}MIM]$. Similarly to

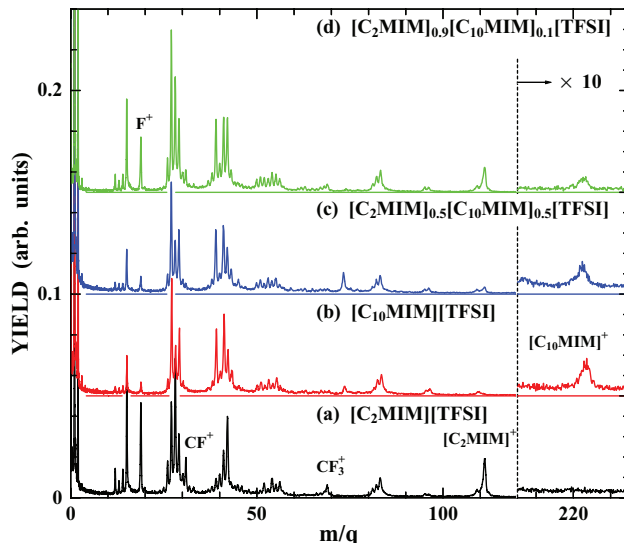


FIG. 12. TOF spectra of the secondary ions emitted from (a) $[C_2MIM][TFSI]$, (b) $[C_{10}MIM][TFSI]$, (c) $[C_2MIM]_{0.5}[C_{10}MIM]_{0.5}[TFSI]$, and (d) $[C_2MIM]_{0.9}[C_{10}MIM]_{0.1}[TFSI]$ during the grazing angle scattering of 0.84 MeV C^+ . The incident angles are (a) $\theta_i = 0.8$ mrad (b) $\theta_i = 1.3$ mrad, (c) $\theta_i = 0.8$ mrad, and (d) $\theta_i = 1.4$ mrad.

$[C_2MIM][TFSI]$, no intact $[TFSI]$ ion was observed. Some fragment ions from $[TFSI]$, such as F^+ and CF^+ are seen but their yields are very low compared to $[C_2MIM][TFSI]$ and no CF_3^+ peak is seen. This is consistent with the surface structure of $[C_{10}MIM][TFSI]$ determined by HRBS (Fig. 6(b)), where $[TFSI]$ anions are covered by the decyl chains of $[C_{10}MIM]$. Thus, the emission of secondary ions originating from $[TFSI]$ is prevented by the decyl chains. The present result demonstrates excellent surface sensitivity of TOF-SIMS. The $[TFSI]$ molecules located at 1 nm from the surface are hardly observed.

Figure 12(c) shows the observed TOF spectrum of the secondary ions emitted from the mixture of $[C_2MIM]_{0.5}[C_{10}MIM]_{0.5}[TFSI]$ during the grazing angle scattering of 0.84 MeV C^+ at $\theta_i = 0.8$ mrad. Surprisingly, the spectrum is almost identical to that of pure $[C_{10}MIM][TFSI]$, except for a small peak of $[C_2MIM]^+$ seen at $m/q = 111$. This suggests the surface is almost completely covered by $[C_{10}MIM][TFSI]$ in contradiction to the HRBS result. The surface molecular composition is estimated from the observed secondary ion yields in the following manner. The measured $[C_2MIM]^+$ yields are $(1.3 \pm 0.2) \times 10^{-2}$ and $(2.3 \pm 0.2) \times 10^{-3}$ ions per incident ion for pure $[C_2MIM][TFSI]$ and $[C_2MIM]_{0.5}[C_{10}MIM]_{0.5}[TFSI]$, respectively. Assuming that the secondary ion yield is proportional to the surface concentration of the relevant molecule, surface fraction of $[C_2MIM]$ in the mixture of $[C_2MIM]_{0.5}[C_{10}MIM]_{0.5}[TFSI]$ is estimated to be 0.18 ± 0.03 . Similarly, the surface fraction of $[C_{10}MIM]$ is estimated to be 1.03 ± 0.16 from the measured $[C_{10}MIM]^+$ yields, which are $(3.4 \pm 0.2) \times 10^{-3}$ and $(3.5 \pm 0.5) \times 10^{-3}$ ions per incident ion for pure $[C_{10}MIM][TFSI]$ and the mixture of $[C_2MIM]_{0.5}[C_{10}MIM]_{0.5}[TFSI]$, respectively. By averaging these fractions, the surface composition is estimated to be $[C_2MIM]_{0.17 \pm 0.03}[C_{10}MIM]_{0.83 \pm 0.03}[TFSI]$.

Figure 12(d) shows the observed TOF spectrum of the secondary ions emitted from the mixture of $[\text{C}_2\text{MIM}]_{0.9}[\text{C}_{10}\text{MIM}]_{0.1}[\text{TFSI}]$ during the grazing angle scattering of 0.84 MeV C^+ at $\theta_i = 1.3$ mrad. The same analysis was performed for this TOF spectrum and the surface molecular composition was determined to be $[\text{C}_2\text{MIM}]_{0.58 \pm 0.04}[\text{C}_{10}\text{MIM}]_{0.42 \pm 0.04}[\text{TFSI}]$.

Finally, there is a small peak at $m/q = 73$ which shows a bit strange behavior. The peak is absent for $[\text{C}_2\text{MIM}][\text{TFSI}]$, low intensity for $[\text{C}_{10}\text{MIM}][\text{TFSI}]$ and highest intensity for $[\text{C}_2\text{MIM}]_{0.5}[\text{C}_{10}\text{MIM}]_{0.5}[\text{TFSI}]$. The peak cannot be assigned but probably originates from trace impurities.

IV. DISCUSSION

Although both HRBS and TOF-SIMS demonstrate surface segregation of $[\text{C}_{10}\text{MIM}]$ for the mixture of $[\text{C}_2\text{MIM}][\text{TFSI}]$ and $[\text{C}_{10}\text{MIM}][\text{TFSI}]$, the degrees of the surface segregation are quite different. The HRBS measurement shows weak segregation, i.e., the fraction of $[\text{C}_{10}\text{MIM}]$ in the topmost molecular layer is determined to be 0.6 ± 0.05 and 0.18 ± 0.02 for $[\text{C}_2\text{MIM}]_{0.5}[\text{C}_{10}\text{MIM}]_{0.5}[\text{TFSI}]$ and $[\text{C}_2\text{MIM}]_{0.9}[\text{C}_{10}\text{MIM}]_{0.1}[\text{TFSI}]$, respectively. On the other hand, the TOF-SIMS measurements show rather strong surface segregation. The obtained $[\text{C}_{10}\text{MIM}]$ fractions are 0.83 ± 0.03 and 0.42 ± 0.04 for $[\text{C}_2\text{MIM}]_{0.5}[\text{C}_{10}\text{MIM}]_{0.5}[\text{TFSI}]$ and $[\text{C}_2\text{MIM}]_{0.9}[\text{C}_{10}\text{MIM}]_{0.1}[\text{TFSI}]$, respectively. As was discussed in the Introduction, similar discrepancies between TOF-SIMS and HRBS/ARXPS were also observed in the previous studies.^{22–24} These discrepancies can be attributed to the extremely high surface sensitivity of SIMS, in other words the difference in the probing depth between HRBS and TOF-SIMS.

As was mentioned above, the yield of secondary ions originating from $[\text{TFSI}]$ anions (e.g., CF_3^+) are much smaller for $[\text{C}_{10}\text{MIM}][\text{TFSI}]$ as compared to $[\text{C}_2\text{MIM}][\text{TFSI}]$. Considering the surface structures of these ILs, the observed large difference in the secondary ion yield can be ascribed to the difference of the position of $[\text{TFSI}]$ in these ILs. In $[\text{C}_{10}\text{MIM}][\text{TFSI}]$, the $[\text{TFSI}]$ anions are located at deeper positions compared to the $[\text{C}_2\text{MIM}][\text{TFSI}]$ and are covered by the decyl chains (see Fig. 6(b)). Emission of the secondary ions originating from the $[\text{TFSI}]$ anions is blocked by these decyl chains. As a result, the yields of these ions are much smaller than those for $[\text{C}_2\text{MIM}][\text{TFSI}]$ as was observed. The same thing happens for the $[\text{C}_2\text{MIM}]$ cations in the mixture. The HRBS measurement suggests that $[\text{C}_2\text{MIM}]$ cations are located at the same depth as $[\text{TFSI}]$ and are covered by the decyl chains (see Fig. 6(c)). Thus the emission of $[\text{C}_2\text{MIM}]$ ions is suppressed. The present result indicates that care must be taken in the quantification of TOF-SIMS. From another viewpoint, the present result demonstrates that TOF-SIMS has excellent surface sensitivity. By combining TOF-SIMS with other quantitative analysis techniques such as HRBS or ARXPS, more detailed information of the surface structure may be obtained. For example, if the surface of the mixture is divided into $[\text{C}_2\text{MIM}][\text{TFSI}]$ and $[\text{C}_{10}\text{MIM}][\text{TFSI}]$ domains, the yield of the secondary $[\text{C}_2\text{MIM}]$ ions should be much

larger than the observed one. Thus we can conclude that surface of the mixture does not have a domain structure.

The present explanation on the discrepancy between TOF-SIMS and HRBS is also applicable for the case of $[\text{C}_4\text{MIM}][\text{TFSI}]_{0.5}[\text{PF}_6]_{0.5}$. The measurement of TOF-SIMS showed strong surface segregation of $[\text{C}_4\text{MIM}][\text{TFSI}]$ ²³ while the HRBS measurement indicates only weak surface segregation.²⁴ This suggests that $[\text{PF}_6]$ anions are located at deeper positions than $[\text{TFSI}]$ in the topmost molecular layer. Such a surface structure was actually observed by HRBS.²⁴

Finally, the origin of the surface segregation of $[\text{C}_{10}\text{MIM}]$ is discussed in terms of surface tension. The surface tensions γ of $[\text{C}_2\text{MIM}][\text{TFSI}]$ and $[\text{C}_{10}\text{MIM}][\text{TFSI}]$ are 36.43 and 31.34 mN/m, respectively.¹¹ The surface free energy per ion pair for $[\text{C}_2\text{MIM}][\text{TFSI}]$ was estimated by $f_2 = \gamma \rho^{-2/3} = 0.129$ eV. This simple formula is not valid for $[\text{C}_{10}\text{MIM}][\text{TFSI}]$ because $[\text{C}_{10}\text{MIM}]$ is a long molecule and its shape cannot be approximated by a cubic. In Sec. III B, the areal atomic density of the topmost layer of $[\text{C}_{10}\text{MIM}][\text{TFSI}]$ was estimated to be 1.07×10^{16} atoms/cm². This corresponds to the areal density of molecular pair of 1.84×10^{14} pairs/cm². Thus the surface free energy per ion pair for $[\text{C}_{10}\text{MIM}][\text{TFSI}]$ is estimated to be $f_{10} = 0.106$ eV. Using these free energies, the surface composition, x_{surf} , of the $[\text{C}_{10}\text{MIM}]$ cation for the mixture of $[\text{C}_2\text{MIM}]_{1-x}[\text{C}_{10}\text{MIM}]_x[\text{TFSI}]$ is given by

$$x_{surf} = \frac{x \exp(-f_{10}/kT)}{x \exp(-f_{10}/kT) + (1-x) \exp(-f_2/kT)}, \quad (2)$$

where k is the Boltzmann constant. The estimated surface composition is 0.71 and 0.21 for $x = 0.5$ and 0.1, respectively. These results are in good agreement with the present results, 0.6 ± 0.05 and 0.18 ± 0.02 .

V. CONCLUSION

The surface structures of the mixtures of $[\text{C}_2\text{MIM}]_{1-x}[\text{C}_{10}\text{MIM}]_x[\text{TFSI}]$ for $x = 0.5$ and 0.1 were observed using HRBS and TOF-SIMS. Both HRBS and TOF-SIMS measurements show the surface segregation of $[\text{C}_{10}\text{MIM}]$ although the observed degrees of the segregation are quite different. The surface fraction x_{surf} of $[\text{C}_{10}\text{MIM}]$ is determined to be 0.6 ± 0.05 and 0.18 ± 0.02 by HRBS for $x = 0.5$ and 0.1, respectively while the results of TOF-SIMS are 0.83 ± 0.03 and 0.42 ± 0.04 . This discrepancy is attributed to the difference in the probing depth between HRBS and TOF-SIMS. Because TOF-SIMS has excellent surface sensitivity, only the molecules located in the outermost position can be observed. Even the molecules being in the topmost molecular layer may not be observed by TOF-SIMS if they are located at the bottom of the topmost layer. From another viewpoint, TOF-SIMS has excellent surface sensitivity. By combining TOF-SIMS and HRBS more detailed information on the surface structure can be obtained.

¹P. Wasserscheid and W. Keim, *Angew. Chem., Int. Ed.* **39**, 3772 (2000).

²R. Sheldon, *Chem. Commun. (Cambridge)* **2001**, 2399 (2001).

³J. Dupont, R. F. Souza, and P. A. Suarez, *Chem. Rev.* **102**, 3667 (2002).

- ⁴P.-Y. Chen and I. W. Sun, *Electrochim. Acta* **45**, 3163 (2000).
- ⁵B. Garcia, S. Lavalle'e, G. Perron, C. Michot, and M. Armand, *Electrochim. Acta* **49**, 4583 (2004).
- ⁶M. Ue, M. Takeda, A. Toriumi, A. Kominato, R. Hagiwara, and Y. Ito, *J. Electrochem. Soc.* **150**, A499 (2003).
- ⁷A. Noda, A. Susan, K. Kudo, S. Mitsushima, K. Hayamizu, and M. Watanabe, *J. Phys. Chem. B* **107**, 4024 (2003).
- ⁸C. Ye, W. Liy, Y. Chen, and L. Yu, *Chem. Commun. (Cambridge)* **2001**, 2244 (2001).
- ⁹H. Niedermeyer, J. P. Hallett, I. J. Villar-Garcia, P. A. Hunt, and T. Welton, *Chem. Soc. Rev.* **41**, 7780 (2012).
- ¹⁰F. Endres and S. Z. El. Abedin, *Phys. Chem. Chem. Phys.* **8**, 2101 (2006).
- ¹¹P. J. Carvalho, M. G. Freire, I. M. Marrucho, A. J. Queimada, and J. A. P. Coutinho, *J. Chem. Eng. Data* **53**, 1346 (2008).
- ¹²S. Baldelli, *Acc. Chem. Res.* **41**, 421 (2008).
- ¹³H.-P. Steinrück, *Phys. Chem. Chem. Phys.* **14**, 5010 (2012).
- ¹⁴T. J. Gannon, G. Law, and P. R. Watson, *Langmuir* **15**, 8429 (1999).
- ¹⁵S. Baldelli, *J. Phys. Chem. B* **107**, 6148 (2003).
- ¹⁶E. Sloutskin, B. M. Ocko, L. Tamam, I. Kuzmenko, T. Gog, and M. Deutsch, *J. Am. Chem. Soc.* **127**, 7796 (2005).
- ¹⁷V. Lockett, R. Sedev, C. Bassel, and J. Ralston, *Phys. Chem. Chem. Phys.* **10**, 1330 (2008).
- ¹⁸S. Caporali, U. Bardi, and A. Lavacchi, *J. Electron Spectrosc. Relat. Phenom.* **151**, 4 (2006).
- ¹⁹O. Höfft, S. Bahr, M. Himmerlich, S. Krischok, J. A. Schaefer, and V. Kemper, *Langmuir* **22**, 7120 (2006).
- ²⁰J. Günster, O. Höfft, S. Krischok, and R. Souda, *Surf. Sci.* **602**, 3403 (2008).
- ²¹K. Nakajima, A. Ohno, M. Suzuki, and K. Kimura, *Langmuir* **24**, 4482 (2008).
- ²²C. Ridings, V. Lockett, and G. Andersson, *Phys. Chem. Chem. Phys.* **13**, 17177 (2011).
- ²³R. Souda, *Surf. Sci.* **604**, 1694 (2010).
- ²⁴K. Nakajima, S. Oshima, M. Suzuki, and K. Kimura, *Surf. Sci.* **606**, 1693 (2012).
- ²⁵F. Maier, T. Cremer, C. Kolbeck, K. R. J. Lovelock, N. Paape, P. S. Schulz, P. Wasserscheid, and H.-P. Steinrück, *Phys. Chem. Chem. Phys.* **12**, 1905 (2010).
- ²⁶K. Kimura, S. Joumori, Y. Oota, K. Nakajima, and M. Suzuki, *Nucl. Instrum. Methods Phys. Res. B* **219–220**, 351 (2004).
- ²⁷K. Nakajima, A. Ohno, H. Hashimoto, M. Suzuki, and K. Kimura, *J. Chem. Phys.* **133**, 044702 (2010).
- ²⁸K. Fujii, T. Fujimori, T. Takamuku, R. Kanzaki, Y. Umebayashi, and S. Ishiguro, *J. Phys. Chem. B* **110**, 8179 (2006).
- ²⁹S. Rivera-Rubero and S. Baldelli, *J. Phys. Chem. B* **110**, 4756 (2006).
- ³⁰T. Iimori, T. Iwahashi, K. Kanai, K. Seki, J. Sung, D. Kim, H. Hamaguchi, and Y. Ouchi, *J. Phys. Chem. B* **111**, 4860 (2007).
- ³¹J. F. Ziegler, J. P. Biersack, and U. L. Littmark, *The Stopping and Range of Ions in Solids* (Pergamon Press, New York, 1985).